Journal of The Electrochemical Society, 2026 **173** 021502

In Situ Neutron Reflectometry and Electrochemical Impedance Spectroscopy Study of Hydrogen Absorption into Copper during Corrosion by Bisulfide

Arthur Situm,[1] Hunter A. Feltham,[1] Jian Chen,[1] Sebastian A. Skaanvik,[1,2] Lars J. Bannenberg,[3] Frans Ooms,[3] Mehran Behazin,[4] Lyudmila V. Goncharova,[5] and James J. Noël[1,2,*,z]

[1]*Department of Chemistry, Faculty of Science, Western University, London, ON, Canada*
[2]*Surface Science Western, Western University, London, ON, Canada*
[3]*Reactor Institute Delft, Delft University of Technology, Delft, Netherlands*
[4]*Nuclear Waste Management Organization, Toronto, ON, Canada*
[5]*Department of Physics, Faculty of Science, Western University, London, ON, Canada*

Sulfide corrosion of Cu is rapid, and hydrogen atoms produced by its cathodic half-reaction could adsorb on the Cu surface and diffuse into the Cu, potentially leading to hydrogen embrittlement. However, in solutions with low concentrations of SH^-, absorption of hydrogen into Cu is not observed by ex situ hydrogen analysis, although it is unclear whether this is due to the lack of absorption, the outgassing of hydrogen from the Cu before it can be measured, or another mitigation mechanism. Herein, hydrogen uptake into Cu and the development of Cu_2S layers during corrosion by SH^- were studied by in situ neutron reflectometry and electrochemical impedance spectroscopy. The method relies on a 4-nm Ti layer beneath 50 nm of Cu to trap hydrogen that may penetrate the Cu. Additionally, elastic recoil detection analysis and Rutherford backscattering spectrometry were used to measure hydrogen. While no increase in hydrogen was detected in either the Ti or Cu layers, a higher concentration of hydrogen was observed in the outer Cu_2S layer (2560 ppm) than in the underlying Cu (244 ppm), demonstrating that bisulfide-driven corrosion does not lead to hydrogen absorption into the Cu. These results have implications for deep geological repositories utilizing Cu corrosion barriers.

 [DOI: 10.1149/1945-7111/ae3649]

Manuscript submitted July 17, 2025; revised manuscript received January 5, 2026. Published January 22, 2026.

Supplementary material for this article is available online

In the fight against climate change, nuclear power is an attractive option, due to its extremely low greenhouse gas emissions.[1] Burial in a deep geological repository (DGR) is widely recognized as being the best option for long-term storage of the resulting used nuclear fuel. In line with this accepted best practice, Canada, Sweden, Finland, France, and Switzerland are in the advanced stages of implementing DGRs while many countries are working through the early planning stages of DGR development.[2,3] Canada's proposed plan for a DGR consists of a multi-barrier system in which used fuel bundles will be sealed into carbon steel containers coated with 3 mm of Cu using electrodeposition and cold spray techniques.[2] Subsequently, these Cu-coated used fuel containers (UFCs) will be placed within a suitable rock formation, surrounded by a bentonite clay buffer to limit the penetration of groundwater and cationic species to the UFC surface.[2]

The possibility of hydrogen absorption into the Cu coatings under DGR conditions, due to hydrogen atoms produced by gamma radiolysis of water or the corrosion of Cu by bisulfide ions (SH^-) generated remotely by the activity of sulphate-reducing bacteria (SRB) beyond the bentonite layer, has received considerable attention.[4–9] The buildup of hydrogen in Cu may result in hydrogen embrittlement, hydrogen blistering, microvoid formation at crystalline imperfections, and a loss in creep ductility.[10,11] It has also been speculated that hydrogen might diffuse through the Cu coatings to reach and affect the adhesion at the Cu/carbon steel interface. Sahiluoma et al. studied friction-stir weld metal specimens of oxygen-free, phosphorus-doped (OFP) Cu that were cathodically charged with hydrogen at various electrochemical potentials ranging from −0.95 to −1.3 V vs the saturated calomel electrode (SCE) in a 1.0 N H_2SO_4 solution with added 10 mg l^{-1} thiourea (NH_2CSNH_2).[12] A threshold potential of −1.10 V SCE^{-1} was found for the marked increase of hydrogen uptake and hydrogen-induced bubble/void formation near the Cu surface.[12] The formation of the hydrogen-induced micro-voids, the most significant form of hydrogen embrittlement of Cu, may not occur in the environments relevant to the final disposal conditions, where the SH^- concentrations are in the range 10^{-7} to 10^{-4} M, as the corrosion potential of Cu (close to the equilibrium potential of the Cu/Cu_2S reaction) is always above the threshold potential of −1.10 V SCE^{-1}.[12–14] Thus, the corrosion potential (E_{CORR}) of the Cu UFC surface will be much higher than the observed cathodic threshold potential for hydrogen-induced void formation, and both the cathodic current density (dependent on the rate of SH^- ion transport to the Cu UFCsurface) and the hydrogen gas pressure will be low.[12]

Forsström et al. studied the absorption of hydrogen into OFP Cu induced by corrosion in deaerated HS^--containing water at 90 °C for 4 weeks (OFP Cu will be used for the dual-walled Cu/cast-iron UFCs in the proposed Swedish and Finnish DGRs).[5] OFP Cu specimens were exposed to slow strain rate tensile (SSRT) straining relevant to the dual-walled UFC design, while simultaneously being exposed to HS^- solutions at concentrations of 1×10^{-3} M or 1×10^{-5} M.[5] While the OFP specimens exposed to the 1×10^{-3} M HS^- solution were found to have higher hydrogen concentrations than the uncorroded OFP specimens, this SH^- concentration is higher than the expected maximum SH^- level (1.2×10^{-4} M) at the proposed Swedish DGR site in Forsmark, and no signs of hydrogen embrittlement were observed.[5] One potential explanation for the lack of embrittlement in the strained 1×10^{-5} M sulfide-exposed specimen may have been the trapping of the hydrogen by the corrosion products rather than absorption into the Cu metal itself, with thermal desorption spectroscopy (TDS) suggesting that Cu_2O particles may be acting as trapping sites.[5] In contrast, when the Cu was exposed to 1×10^{-5} M HS^- solution in the absence of SSRT straining, less hydrogen absorption was observed than in the uncorroded OFP Cu. This result indicates that the outgassing of hydrogen from the OFP Cu was greater than the absorption of hydrogen into the OFP Cu from SH^-

*Electrochemical Society Fellow.
[z]E-mail: jjnoel@uwo.ca

corrosion.[12] However, the study relied on hydrogen thermal desorption spectroscopy (TDS), which, while having a low detection limit for hydrogen (0.02 wt ppm), involves the ex situ analysis of large sections of the specimen, with ~34 mm^3 of each SSRT specimen used for TDS analysis. While very adept at detecting changes in the bulk of the specimen, TDS lacks surface sensitivity, and may overlook hydrogen absorption at the brittle/porous Cu_2S surface film. The absorption of hydrogen into the Cu_2S film may prevent its absorption into the bulk Cu, the film potentially acting as a partial sink for hydrogen.

In the study of corrosion, neutron reflectometry has emerged as a powerful technique, due to its ability to enable in situ experiments and measure changes in layer thickness in the range of 3−100 nm.[15] Previous applications of NR for studying corrosion have included studying the development of passive films in water, the effectiveness of corrosion inhibitors, and atmospheric corrosion.[16–26] Situm et al. have previously investigated the absorption of hydrogen on a Cu-coated Si wafer with a thin Ti adhesion layer using in situ NR and electrochemical impedance spectroscopy (EIS).[9] Hydrogen was generated by cathodically polarizing the surface of the Cu to −1300 mV (vs SCE), far more negative than the corrosion potential of Cu (−925 mV (vs SCE)) observed in an anoxic solution containing 5×10^{-4} M Na_2S.[14] They demonstrated that hydrogen produced by cathodic polarization of the Cu diffuses rapidly through the Cu and accumulates in the Ti layer until the Ti is saturated, with no buildup of hydrogen in the Cu layer or at the Cu/Ti interface detected.[9] They also observed that only a maximum of 3.2 at% of the hydrogen atoms produced diffused through the Cu layer, suggesting an upper limit to the uptake efficiency of hydrogen.[9]

While these results indicate that hydrogen absorption is unlikely to lead to the failure of the Cu barrier under anticipated DGR conditions, the absorption and diffusion rate of hydrogen may be significantly altered by the formation of the porous Cu_2S film on the Cu surface as a result of corrosion in SH^- solution.[2,4,27] This research aims to measure the corrosion of Cu by SH^- in situ and any resulting hydrogen absorption and permeation occurring in the bulk Cu or the brittle/porous Cu_2S film. NR and EIS were used to study the development of the Cu_2S film in situ on a Cu-coated Si wafer with a Ti adhesion layer. Following NR, corrosion testing in SH^- solution, elastic recoil detection analysis (ERDA) and Rutherford backscattering spectrometry (RBS) were performed to measure the concentration of hydrogen and sulfur in the Cu/Ti film as a function of depth. The current work is the first study that examines the role of the brittle/porous Cu_2S film in the process of hydrogen absorption into Cu during corrosion in SH^--containing solution.

Experimental

Specimen fabrication.—Electron-beam physical vapour deposition (EBPVD, Angstrom Engineering) was used to deposit a 4-nm film of Ti (Angstrom Engineering, 99.995%) followed by a 50-nm film of Cu (Kurt Lesker, 99.99%) onto a 100-mm-diameter, 6-mm-thick, polished silicon wafer ((111), Wafer World) and a 100-mm-diameter, 0.5-mm-thick polished silicon wafer ((111), Wafer World). The 6-mm-thick silicon wafer previously had Ti and Cu coatings that were chemically removed prior to depositing the new films using EBPVD. The EBPVD device automatically determined the thickness of the coating by quantifying the mass added to an internal quartz crystal microbalance (QCM). The choice of a 6-mm-thick wafer was to prevent the bending of the specimen during NR measurements, as well as to transport the neutron beam through the silicon, while the 0.5-mm-thick wafer was used as a control specimen for ERDA and RBS analysis. A focused ion beam (FIB) cut was made, and a scanning electron microscopy image of the specimen cross-section was collected from the 0.5-mm-thick Ti-Cu-coated specimen to demonstrate the flatness of the films deposited using EBPVD (see supplemental information (SI) Fig. S1). The specimens were stored within a desiccator when not in use.

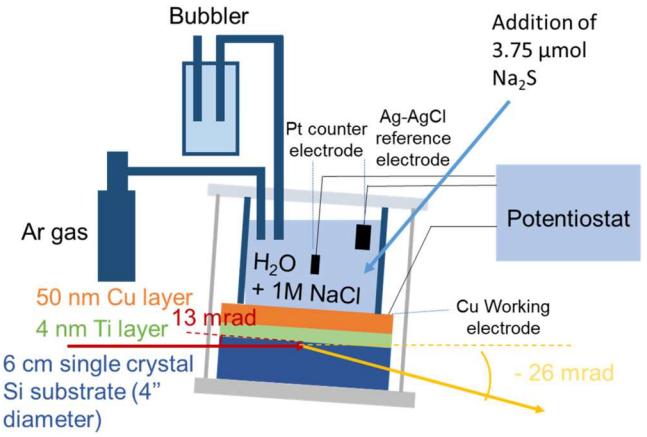

Figure 1. A schematic of the electrochemical cell used for the in situ NR experiments. The bubbler wasused to prevent air ingress back into the NR electrochemical cell.

In situ measurements on the Cu-Ti thin film by NR and EIS.—The thin-film Cu-Ti specimen was exposed to a deaerated saline solution containing Na_2S, and in situ NR, EIS, and E_{CORR} measurements were performed to study the corrosion of the Cu and any resulting hydrogen absorption into the Cu. The Cu-Ti specimen was used as the working electrode in a three-electrode electrochemical cell (Fig. 1). Electrochemical measurements were performed using an Autolab PGSTAT204 equipped with the EIS module (Metrohm). An electrical connection to the Cu coating was made using a pure Cu ribbon tucked under the butyl rubber O-ring used to create a seal between the polytetrafluoroethylene body of the cell and the Cu-Ti thin-film specimen. An area of 65 cm^2 of Cu was exposed to the electrolyte. A saturated Ag/AgCl reference electrode (potentials are quoted on this scale) and a platinum plate counter electrode were used. The electrolyte was a 0.1 M NaCl solution sparged with ultra-high-purity argon (99.999%) before and during the experiment. Upon addition of the argon-sparged electrolyte but prior to the start of the experiment, a potential of −400 mV was applied to reduce the air-formed oxides while the solution continued to be argon-sparged. During the Na_2S exposure experiment, the E_{CORR} was monitored, with 3.75 µmol Na_2S added after 5 min resulting in a 5×10^{-6} M SH^- solution. Given that there was approximately 46 µmol of Cu present in the exposed area of the Cu-Ti thin-film specimen, around 16% of the Cu was expected to be consumed, assuming that all Na_2S reacted with Cu to form Cu_2S. EIS measurements were performed in triplicate continuously throughout the 51-hour experiment, with E_{CORR} measurements made in between.

The NR measurements were performed at the ROG Neutron Reflectometer of the Reactor Institute Delft, Delft University of Technology, The Netherlands. The double disc chopper was set to a frequency of 17.7 Hz, with an interdisc distance of 0.280 m, resulting in a wavelength resolution of $\Delta\lambda/\lambda \approx 2.5$. The incident angle was set to 13 mrad. The neutron spectral range $0.13 < \lambda < 1.3$ nm was used, leading to a Q-range of $0.14 < Q < 1.2$ nm^{-1}. A first slit of 1.8 mm and a second slit of 1.2 mm were used, of which the latter was positioned approximately 150 mm before the specimen, resulting in a neutron beam footprint of 80×40 mm^2/95×40 mm^2 (umbra/penumbra) and a resolution of $\Delta Q/Q \approx 0.045$. The neutrons were detected using a ^{3}He detector. The NR data were fitted using GenX 3.6.3.[28] to obtain estimates for the thickness, scattering length, and roughness of each layer. The specimen was divided into three layers on top of a substrate: a Ti layer, a Cu layer and an interfacial layer, while the ambient material was H_2O. During fitting, the roughness of the Ti and Si substrates was kept constant, at 0.3 and 0.5 nm, respectively, as derived from previous experiments. The Ti and Cu layers had theoretical densities of 4.51 g cm^{-3} and 8.96 g cm^{-3}, respectively. The densities of the substrate and the H_2O were kept

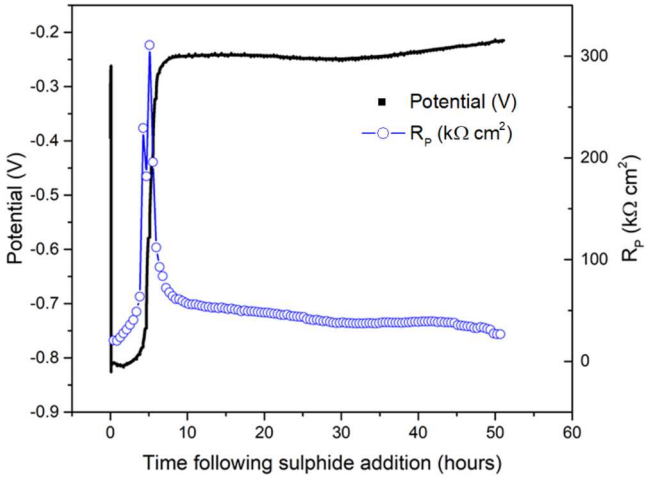

Figure 2. Evolution of corrosion potential and polarization resistance with the immersion time after SH^- addition.

fixed at their respective theoretical values (i.e., Si 2.33 g cm^{-3}, and H_2O 1.00 g cm^{-3}) during fitting. We note that neither keeping the roughness of the Ti or Si layer fixed at a constant value nor allowing it to vary during model fitting significantly affected the conclusions. When kinetic measurements were performed, a time resolution of 1 h was chosen as a compromise between achieving good measurement statistics and obtaining high time resolution.

Post-experimental specimen handling and scanning electron microscope (SEM) imaging.—Following the SH^- exposure experiment, the NR electrochemical cell was disassembled, and a photograph of the thin-film Cu-Ti specimen was taken (see Fig. S2). The thin-film Cu-Ti specimen was then rinsed with deionized (DI) water and dried with a jet of Ar gas before being stored in a desiccated environment to minimize specimen corrosion when not in use. The specimen was sectioned using a water-cooled diamond saw and divided into pieces approximately 1 cm × 2 cm in size, which were then used for SEM imaging, ERDA, or RBS analysis. SEM imaging was performed using a Hitachi SU3900 Large Chamber Variable Pressure SEM at Surface Science Western (SSW).

Elastic recoil detection analysis (ERDA) and Rutherford backscattering spectroscopy (RBS) measurements..—ERDA was used to quantify the hydrogen depth profile of the Cu/Ti/(111) Si layers on both the control specimen and the specimen that had undergone the in situ neutron scattering experimentation. RBS was performed on the thin-film Cu-Ti specimen to verify the homogeneity of the electron-beam-deposited Ti and Cu on Si (111) and to quantify any impurities, such as sulfur. ERDA and RBS were performed at the Western Tandetron accelerator facility using a 30 keV He^+ beam, normal geometry, with the RBS Si barrier detector mounted at 160°, in Cornell geometry.[29] At 30° normal to the beam was an ERDA detector covered in a thin film of Mylar foil to impede non-hydrogen scattering and to avoid the need for incident beam deconvolution. The energy of the recoiled ion in each experiment decreased due to several shared factors, including elastic or inelastic collisions, scattering cross-sections, and stopping cross-sections.[30] A control standard was used to quantify the ERDA layer profile by measuring a polyimide Kapton specimen to generate a standard energy for the elastic recoil of the surface and integrated hydrogen under experimental conditions. A standard for the known hydrogen atomic percent in a repeating imide structure was used to quantify a uniform hydrogen profile and allowed for the comparison to any hydrogen dissolved in either the Cu or Ti structures. By assessing the areal and atomic densities of Ti and Cu elements near the specimen surface, measurements were used to ascertain the thickness of their respective layers.[31] Due to the non-ideal geometry of the RBS detector, made

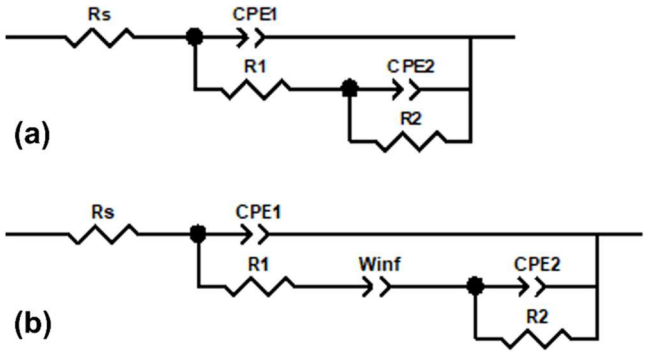

Figure 3. Equivalent circuits used to fit the EIS spectra recorded on a Cu electrode after immersion in de-aerated 5 × 10^{-5} M Na_2S + 0.1 M NaCl solution for (a) <5 h; and (b) >5 h, in which R_s is the solution resistance, CPE_1 is the constant phase element representing the double layer capacitance, R_1 is the charge transfer resistance, CPE_2 and R_2 represent the adsorption layer capacitance and resistance, respectively, and W_{inf} is the infinite Warburg impedance corresponding to the SH^- diffusion in the solution or the pores in the Cu_2S film.

necessary by spatial limitations within the vacuum chamber and the low energy requirements of ERDA, RBS had a lower level of certainty in these measurements than in the RBS spectrum performed without ERDA coupling. To align the edges of the ERDA spectra, the hydrogen profile of the adventitious carbon surface adherence layer was manually aligned for each spectrum. For each experiment, three different spots on the surface were tested with both ERDA and RBS to determine the homogeneity of the deposited layers and the hydrogen depth profile. Differences in the integrated peak areas were less than 3% for ERDA and RBS for each spot on the same surface. The Simulation of Nuclear Reaction Analysis (SIMNRA) program was utilized for fitting ERDA and RBS spectra, and the near-surface profile of the material was accurately generated.[32] The statistical uncertainty of the resultant spectra as a function of depth is well-known and considered when simulated using SIMNRA.

Results

Electrochemistry of a Cu-Ti thin film.—E_{CORR} and the polarization resistance (R_P) values extracted from EIS fitting are shown in Fig. 2 as a function of time following the cathodic cleaning (−400 mV vs sat. Ag/AgCl). The E_{CORR} was observed to drop sharply from around −250 mV to −825 mV upon the addition of Na_2S, in line with SH^- either directly reacting with exposed Cu and the air-formed oxide residues to form Cu_2S, or diffusing through the pores in the air-formed oxides and reacting with Cu to deposit Cu_2S, leading to the negative shift in E_{CORR}.[33,34] Since the SH^- flux to the Cu surface was increased by introducing partially convective conditions (by Ar sparging), it initially accelerated the formation and growth of the Cu_2S film, resulting in a lower initial R_P value (∼20 kΩ cm^2) at ⩽1 h of immersion.[13,14] In the early stage of the experiment, the increase in the SH^- flux may have changed the structure and properties of the Cu_2S film, facilitating the initial formation of a dense Cu_2S layer whose growth was controlled by Cu (I) diffusion in the film.[35] However, since the lowest frequency of EIS measurements in the present study was 0.01 Hz, the low-frequency response arising from Cu(I) diffusion was not detected by EIS (i.e., the measurement frequency was not low enough).[14] To model this more dense Cu_2S film when performing EIS fitting, the equivalent circuit shown in Fig. 3a, lacking a short Warburg impedance element associated with Cu(I) diffusion in the film, was used, with an example fitting shown for the EIS spectrum collected after 15 min (see Fig. 4). The formation of the denser Cu_2S resulted in an increase in R_p leading up to 5 h of exposure time.[21]

Due to the large Pilling-Bedworth ratio of Cu_2S (i.e., 2), its rapid growth increased the film growth stress (compressive), leading to film rupture and a decrease in R_P at >5 h.[36] The results of density

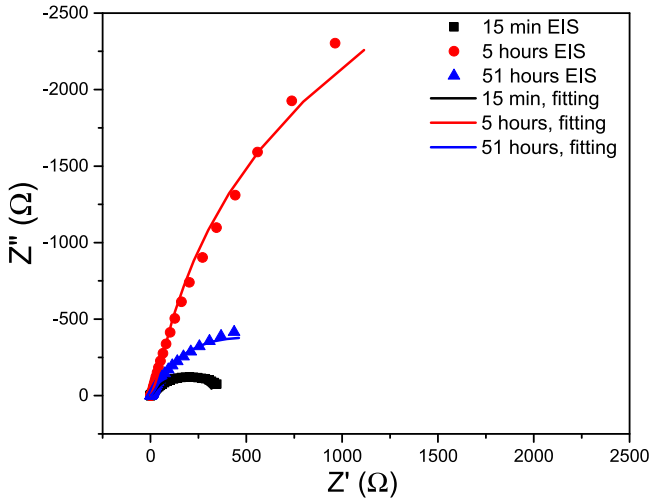

Figure 4. Examples of EIS fitting using the equivalent circuits shown in Fig. 3.

functional theory calculations are consistent with an expectation that a porous and non-adherent Cu_2S film will form on Cu due to a significant geometric mismatch between the Cu substrate and the Cu_2S film.[37] The growth of a porous Cu_2S film was controlled by SH^- transport in the solution or the pores in the Cu_2S film.[13] Fitting of EIS spectra collected after 5 h was performed using the typical equivalent circuit for modelling porous Cu_2S films, with the infinite Warburg element representing the SH^- diffusion process (see Figs. 3b and 4).[13,14] This rapid film growth and the large exposed surface area also accelerated SH^- consumption, leading to the depletion of SH^- at the surface and, thus, the positive shift in E_{CORR}.[35,38] The development of a porous film is consistent with SEM imaging after the experiment, as shown in Fig. S3. At a longer immersion time (i.e., >6 h), where SH^- was extremely depleted, the growth of the Cu_2S film was slow and controlled by SH^- diffusion in the solution.[13] Under these circumstances, the E_{CORR} was shifted positively, and the R_P had minor changes (~40 kΩ cm^2 after 10 h).

In situ NR of bisulfide-exposed Cu-Ti thin films.—NR reflectograms collected from the Cu-Ti thin films before and at various times after Na_2S addition, as well as the modelled fits, are shown in Fig. 5a. One of the major advantages of NR is the nuclei-specific nature of the technique, which arises from the variations in the scattering length of each nucleus.[9] By combining the coherent neutron scattering length from each element and isotope with the weighted average number density of nuclei, a scattering length density (SLD) can be modelled, and an SLD profile can be generated as a function of depth.[9] The SLD profile for the Cu-Ti thin film is shown in Fig. 5b, with the depths associated with the Si, Ti, Cu, interfacial region, and H_2O marked. One notable difference between this work and the previous in situ NR study examining electrochemical-driven hydrogen absorption in Cu[9] is the lack of change in the SLD of the Ti layer. Ti is known to take up hydrogen readily, with the formation of Ti hydride in the Ti layer acting as a measure of hydrogen permeation through the Cu.[9,39] The lack of alteration in the SLD of the Ti layer in the present study indicates a lack of hydrogen permeation through the Cu layer. In contrast, a large change in SLD was observed at the Cu/electrolyte interface, corresponding to multiple simultaneous processes stemming from S, O, and H having lower scattering lengths than Cu. In the inner interfacial region, the observed drop in SLD was likely due to the increase in porosity of the Cu_2S film, the ingress of water into the porous Cu_2S film, the formation of SH groups within the film, and, to a lesser extent, hydrogen absorption into the film. It is consistent with the electrochemical results in Fig. 2. Conversely, the slight rise in SLD observed in the outer interfacial region may have been due to

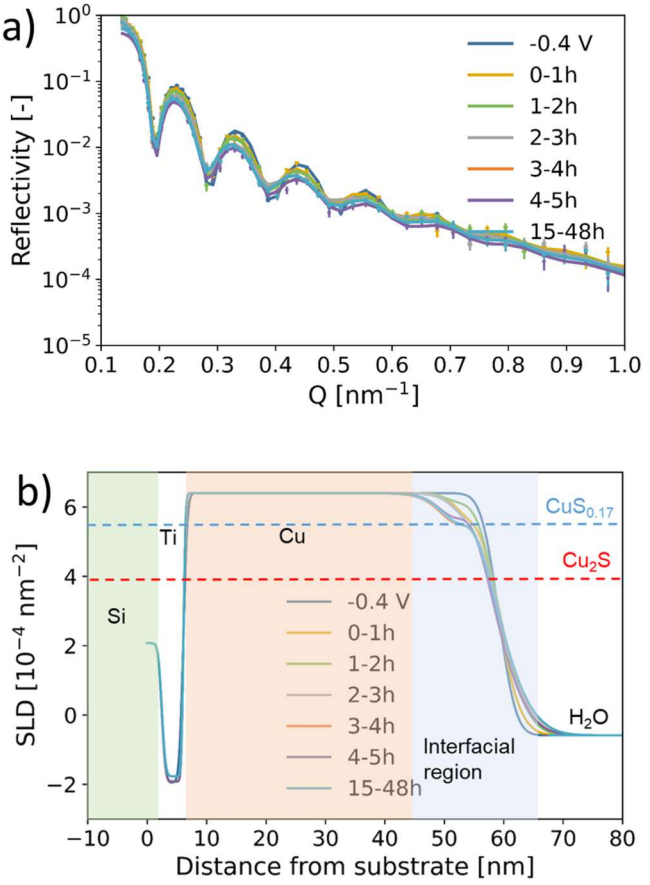

Figure 5. In situ neutron reflectometry results on the Cu-Ti thin film prior to the introduction of Na_2S (−0.4 V $_{vs\ sat.\ Ag/AgCl}$ applied potential) and at several times following the introduction of Na_2S. Panel (a) shows the neutron reflectograms, where the points represent the measured data and the continuous curves the model fits to the data; the corresponding real-space SLD profiles are displayed in panel (b). The legend indicates the time window of the kinetic measurements following the addition of SH^-. The period between 15 and 48 h did not yield any significant change, hence the data were summed to improve the measurement statistics.

the expansion of the Cu_2S film into the volume initially only occupied by water, owing to the large Pilling-Bedworth ratio. The roughness of the interfacial region was found from modelling the SLD as a function of SH^- exposure time and is shown in Fig. 6, indicating a steady rise in roughness of the interfacial region from 20 nm to 53 nm between 1 and 4 h of exposure to SH^-. This rise in roughness is in line with the interpretation that the rise in SLD in the outer interfacial layer is due to the expansion of a Cu_2S film with a higher roughness than that of the Cu layer. Also indicated in Fig. 5 is the theoretical SLD value of Cu_2S. A comparison of the theoretical and actual SLD values shows that a portion of the interfacial region had a higher SLD, indicating a Cu:S ratio higher than 2. A portion of the interfacial region had a lower SLD, suggesting the ingress of aqueous solution (which has a negative SLD) into the porous Cu_2S film. While the drop in SLD across the interfacial region was continuous, starting at 3–4 h, a partial plateau can be observed to have developed between around 50 and 55 nm, as indicated on Fig. 5b. Little change in the SLD was observed in the Cu region, suggesting little (<2 at%) hydrogen penetration into the Cu, although the limited solubility of H in Cu is the reason a Ti underlayer was used to measure H penetration.

Post-Na_2S exposure ERDA and RBS results.—To investigate the changes in composition resulting from the corrosion experiments, ERDA and RBS measurements were performed on both the corroded and control specimens. Fig. S4 shows a representative ERDA

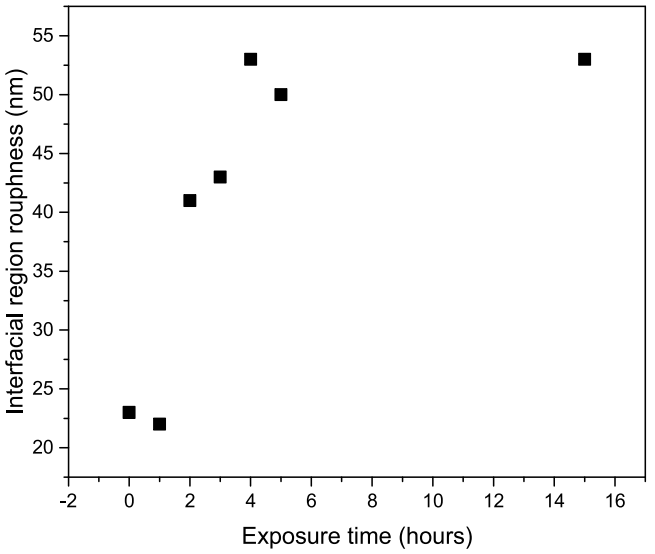

Figure 6. Roughness of the interfacial region calculated from model fits of reflectograms shown in Fig. 5 as a function of immersion time after SH^- addition. The period between 15 and 48 h did not yield any significant change, hence the data were summed to improve the measurement statistics.

Table I. ERDA measured total hydrogen concentrations of Cu specimens with a standard error of ± 10 ppm by weight.

Specimen	Total H (ppm by weight)	H (ppm by weight) in the outer 12 nm	H (ppm by weight) beneath the outer 12 nm
Control	940	1240	410
Specimen corroded in bisulfide solution	990	2560	240

spectrum collected from a control Cu/Ti/Si (111) specimen and the Cu/Ti/Si (111) specimen after use in the corrosion experiments in SH^- solution, with three unique measurements performed a minimum of 10 mm apart. The percent difference between hydrogen profiles at corresponding locations within individual specimens was less than 3% for both the control and in situ neutron scattering specimens, indicating similar uncertainties across multiple sample points in each specimen. The differences between optically differing heterogeneous regions on the SH^--exposed specimen were analyzed with ERDA, and the difference in the depth profiles was found to be within the bounds of the inherent uncertainty of ERDA experiments.

We developed a hydrogen concentration layer structure for each specimen by simulating ERDA data, as shown in the hydrogen depth profile obtained from ERDA comparing the areal concentration of H (in cm^{-2}) as a function of depth in Cu/Ti/(111) Si for both control and post-experimental specimens. RBS was used to identify the location of the Cu/Ti interface. These results indicate a significantly higher hydrogen concentration in the surface layer of the specimen corroded in SH^- solution, with the hydrogen in the outer 12 nm also increasing from 1240 to 2560 (± 10) ppm by weight (see Table I). The specimen corroded in SH^- solution showed a lower concentration of H in the subsurface.

Analysis of the RBS data revealed the presence of a S inclusion in the specimen corroded in SH^- solution, which was absent in the control specimen, as seen in the RBS spectra shown in Fig. S5. The RBS depth profiles, simulated via SIMNRA, describe a depth profile that aligns with those of the earlier ERDA specimens. In the case of the specimen corroded in SH^- solution, the broadening of the Cu peak suggests a slightly thicker Cu layer, while the tailing in the

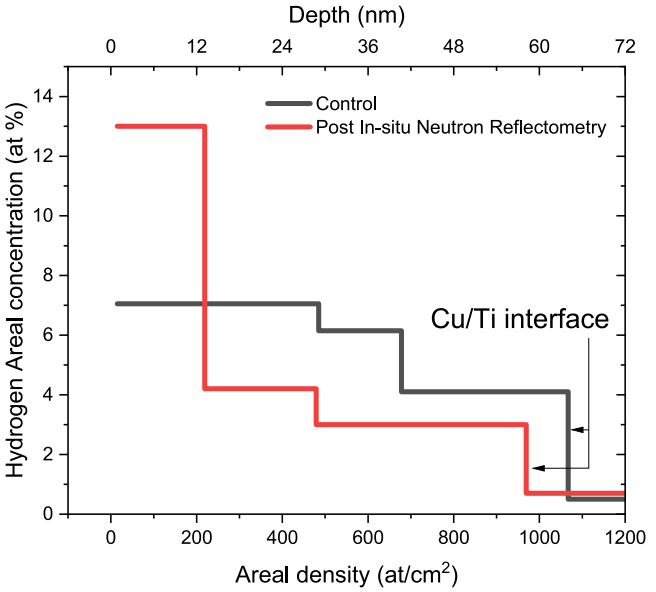

Figure 7. Hydrogen depth profile obtained from ERDA, comparing the areal concentration of H (in cm^{-2}) as a function of depth in Cu/Ti/(111) Si for both control and post-experimental specimens. RBS was used to identify the location of the Cu/Ti interface.

channel 700–800 region is attributed to the roughened interface between layers. This phenomenon is likely the result of reusing the underlying silicon wafer and the influence of the cleaning process to remove traces of the previous experiment impacting the surface morphology. This interpretation is further substantiated by the slope of the Si edge, which displays the same characteristic broadening behaviour. Despite this, the features within the channel 350–400 range do match the anticipated pattern of the oxide layer due to the exposure of the specimen to air following the end of the in situ NR experiment, confirming the distribution of oxide within the simulated dataset. A clear S peak emerged subsequent to in situ neutron scattering within the channel 600–670 region. SIMNRA simulations indicate that there was 31.6 at% of S in the outermost 10 nm, dropping to 13 at% S in the subsequent 40 nm of the specimen. The RBS data align with the ERDA dataset and establish a consistent layer structure that effectively models both data sets.

RBS was used to calculate overall layered stacks, with the control specimen found to be 4 nm $CuO_{0.05}C_{0.2}$/54 nm $CuO_{0.03}$/3 nm $TiO_{0.1}$/Si (111), and the specimen corroded in SH^- solution found to be 10 nm $CuO_{0.04}S_{0.31}$/12 nm $CuO_{0.05}S_{0.16}$/37 nm $CuO_{0.04}$/4 nm $TiO_{0.1}$/Si (111) (the ∼2-nm adventitious carbon layers have been omitted). While the first 4 nm of the control specimen was found to have trace C and slightly higher O, there was no observed difference in hydrogen content between the first 4 nm of the control and the subsequent 20 nm, as shown by the ERDA results in Fig. 7. The inclusion of O and other impurities in the Cu and Ti likely originated from the EBPVD Cu and Ti deposition process, due to a non-ideal vacuum.[22] Additionally, the presence of O in the Cu_2S film likely originated from the partial oxidation of the specimen corroded in SH^- solution following the exposure of the specimen to air at the end of the experiment, prior to drying.

Discussion

In situ NR and EIS were used to study hydrogen uptake into a 50-nm Cu thin film via corrosion in SH^- solution. A 4-nm layer of Ti under 50 nm of Cu was used to trap any hydrogen that permeated the Cu layer. The method presented herein has several distinct advantages over commonly used techniques for measuring hydrogen. First, it is an in situ technique, which allows the absorption of hydrogen to be studied as a function of time or applied potential. Moreover, the method is able to differentiate between hydrogen absorbed into the

metal, surface-adsorbed hydrogen, or hydrogen trapped in the corrosion product film, although NR can not differentiate between hydrogen dissolved/trapped in Cu_2S or nano-particulates decorated on the Cu_2S surface which are converted from $Cu(SH)_2^-$ complexes and Cu_3S_3 that transports from the corroding front to the Cu_2S film/electrolyte interface.[40] This is essential because the latter two types of hydrogen are not expected to lead to a reduction in mechanical performance. In addition, Ti is an effective hydrogen trap that prevents hydrogen from offgassing under vacuum conditions, making hydrogen detection easier. Lastly, the sensitivity of the technique is very high, due to the extremely thin layer of Ti, only 4 nm, despite the low detection limit within the Ti layer itself (2 at%).[9] The challenge of relating surface concentrations of hydrogen to bulk concentrations is especially difficult for specimens corroded in SH^- solution, where the amount of hydrogen absorption is expected to be small and the hydrogen may be trapped in the porous Cu_2S film.

NR measurements tracked the formation of the porous Cu_2S film through the drop in SLD observed in the Cu layer in the outermost 22 nm of the specimen (referred to as the "interfacial region" in Fig. 5b). In addition, the expansion of the specimen film by around 7 nm is in line with the large Pilling-Bedworth ratio of Cu_2S (i.e., 2). These observations are in close agreement with the RBS analysis, which found a ratio of Cu to sulphur of 3.2Cu:S in the outer 10 nm of the specimen, followed by a ratio of 6.3Cu:S in the following 12 nm. The remainder of the Cu was not observed to have reacted with SH^- by either RBS or NR. The 6.3Cu:S layer, as measured by RBS analysis, corresponds with the portion of the interfacial region measured by in situ NR observed to have developed a partial plateau in the SLD 3 h after the introduction of SH^-, corresponding with a composition of 5.9Cu:S (see Fig. 5) which agrees well with the results obtained from RBS at the same depth range (i.e., 6.3Cu:S). The development of this 5.9Cu:S layer corresponded with the sharp rise in R_p and the start of the increase in E_{CORR} (see Fig. 2). The rise in E_{corr} was associated with the majority of the SH^- having reacted with Cu, which is confirmed by the lack of changes in SLD in all in situ NR measurements conducted after 3 h. Moreover, the sharp rise in R_p between 3 and 4 h following the addition of SH^- to the solution was due to the development of a compact Cu_2S film, prior to the development of porosity corresponding with the sharp drop in R_p values after 5 h. While the 5.9Cu:S layer may have been compact initially, the lack of observable change in the SLD of the specimen post 4 h shows that the transition from a compact to a porous Cu_2S film is not observable with NR, potentially due to NR having no resolution in the x-y plane of the specimen and the volume fraction of the surface film occupied by pores being too small to induce a measurable change in the SLD averaged over the entire neutron beam footprint.

Micro/macro-galvanic corrosion has previously been observed at higher concentrations of SH^-.[40] However, experiments previously performed at 5×10^{-5} M Na_2S have shown that the film growth kinetics are linear and do not show micro/macro-galvanic corrosion effects, which is in line with the consistent results observed from RBS and ERDA measurements collected across the surface of the specimen corroded in SH^- solution.[13,40] Overall, this result shows that with very low fluxes of SH^-, the transition of the Cu_2S film from compact to porous is inevitable.

In this study, no evidence of hydrogen absorption into the Ti layer by NR following the addition of SH^- was observed, suggesting that hydrogen produced by proton reduction (from SH^- reaction with Cu) rapidly recombines into H_2 gas and desorbs from the Cu_2S surface. If any hydrogen permeated through the Cu layer, a hydrogen concentration in the Ti layer above the 2 at% detection limit of NR would be expected. The lack of hydrogen accumulation in the Ti layer and a lower hydrogen level at the subsurface layer than observed in the control specimen were further confirmed by ERDA (see Fig. 7 and Table I). The lack of hydrogen absorption is in contrast to the previous in situ NR study, which showed a rapid penetration of hydrogen through the Cu layer and absorption of hydrogen into the Ti layer, driven by cathodic polarization.[9] That work found a maximum absorption efficiency (i.e., hydrogen generated through the hydrogen evolution reaction (HER) that diffused through the Cu into the Ti) of 3.2%. This lack of hydrogen at low SH^- concentrations is in agreement with the results found by Forsström et al., who showed no increase in the hydrogen concentration in OFP Cu exposed to 1×10^{-5} M Na_2S. However, the ERDA performed in this study shows a buildup of hydrogen in the outermost Cu_2S layer (3.2Cu:S). The 3.2Cu:S layer showed a hydrogen concentration of 2560 ppm wt% compared with an average of 244 ppm wt% in the control specimen (see Table I). This result suggests that the hydrogen generated on the top of the 3.2Cu:S layer may become trapped within this layer or form CuSH, mitigating H absorption into the bulk Cu. More generally, the absorption of hydrogen into Cu is more efficient when that hydrogen is adsorbed to the bare metal during cathodic polarization.[9] One potential explanation for this is that when the cathodic reactions are separated from the metal by a conducting film, such as Cu_2S,[12] hydrogen absorption into Cu may be mitigated.

While Forsström et al.[5] showed that the gauge sections of OFP Cu specimens exposed to a 1×10^{-3} M SH^- solution buffered with Na_2HPO_4 and NaH_2PO_4 had a similar hydrogen content to their thread sections and claimed that hydrogen intake at these sections attributes to the absorption of hydrogen into the bulk Cu, the retention effect of the Cu_2S layer on hydrogen absorption may explain the lack of hydrogen absorption at 1×10^{-5} M Na_2S.

Under DGR conditions, once all trapped oxygen is consumed by aerobic microbial activity, container oxidation, and reactions involving Fe(II) and sulfide minerals in the bentonite, anaerobic conditions will be established. Under these conditions, SH^- remotely produced by the activity of sulfate-reducing bacteria and the dissolution of sulfide-containing minerals, is expected to be low (typically 10^{-7} to 10^{-4} M).[2] The initial SH^- concentration ($[SH^-]$) used in our study (5×10^{-6} M) is therefore representative, particularly for Canadian DGR conditions, where groundwater $[SH^-]$ typically ranges from 10^{-7} to 10^{-6} M.[2] Our in situ NR and ERDA results (Fig. 6 and Table I) demonstrate that hydrogen produced via proton reduction rapidly desorbs from the Cu_2S surface and is released as H_2. Long-term hydrogen permeation is therefore not expected; however, further hydrogen analyses of Cu specimens exposed to anoxic SH^- solutions at various concentrations over extended durations are needed to confirm this.

External dose rates from γ-radiation penetrating Cu UFC walls will be very low, and both calculations and experiments have demonstrated that γ-radiation–induced corrosion will be negligible.[2,41,42] Although oxide formation on the Cu UFC during the initial oxic stage of the DGR and subsequent changes in groundwater chemistry (e.g., $[SH^-]$, $[Cl^-]$, and other species such as SO_4^{2-} and HCO_3^-/CO_3^{2-}) could change the morphology, structure, and properties of the Cu_2S film, they are not expected to alter the nature or location of the cathodic reaction.[33,43] Whether such changes in Cu_2S film characteristics could affect the hydrogen adsorption/desorption behaviour remains an open question and requires further investigation. Future work could include performing experiments wherein Cu is exposed to SH^- solutions of various concentrations, followed by RBS and ERDA to determine whether this mitigation effect on hydrogen absorption depends on the morphology, structure and porosity of Cu_2S film and the amount of hydrogen produced during film formation.

Conclusions

In this study, the possibility of hydrogen uptake into Cu and the development of Cu_2S layers during SH^- corrosion were studied by in situ NR and EIS, as well as by ex situ RBS and ERDA.

- The Cu_2S film developed on the surface of the Cu thin film due to exposure to a low concentration of SH^- was initially observed to be compact before it transitioned to porous
- The transition of the Cu_2S film from compact to porous occurred without any alteration in NR reflectograms, suggesting

that the transition from compact to porous occurs via small cracks in the Cu_2S layers

- No hydrogen absorption into either the Ti or Cu layer was detected by either NR or ERDA, but the presence of hydrogen in the outer Cu_2S layer (average 3.2Cu:S ratio) was detected and found to be higher than in the as-prepared specimen

Acknowledgments

This work was jointly funded by the Natural Sciences and Engineering Research Council of Canada (NSERC) and the Nuclear Waste Management Organization through Alliance Grant ALLRP 561193–20. An NSERC postdoctoral fellowship (PDF) supported Dr Arthur Situm during a portion of this study. We gratefully acknowledge Tim Goldhawk and Todd Simpson at Western Nanofabrication facility for specimen preparation, Jack Hendriks for his valuable help with RBS analysis at the Tandetron Accelerator Facility and Michel Thijs for support with the NR measurements. Funding for RBS was provided by NSERC Discovery Grants RGPIN-2020–06679 and RGPIN-2023–05794.

ORCID

Arthur Situm https://orcid.org/0000-0002-4329-290X
Hunter A. Feltham https://orcid.org/0000-0003-4854-4368
Jian Chen https://orcid.org/0000-0003-4021-7127
Sebastian A. Skaanvik https://orcid.org/0000-0002-5302-8221
Lars J. Bannenberg https://orcid.org/0000-0001-8150-3694
Frans Ooms https://orcid.org/0000-0002-5704-6582
Mehran Behazin https://orcid.org/0000-0001-5245-4256
Lyudmila V. Goncharova https://orcid.org/0000-0001-8085-9859
James J. Noël https://orcid.org/0000-0003-3467-4778

References

1. D. Weisser, *Energy*, **32**, 1543 (2007).
2. D. S. Hall, M. Behazin, W. Jeffrey Binns, and P. G. Keech, *Prog. Mater Sci.*, **118**, 100766 (2021).
3. J. A. Cherry, W. M. Alley, and B. L. Parker, "Geologic disposal of spent nuclear fuel: An earth sciences perspective." *The Bridge (National Academy of Engineering)*, **44** (Spring), 51 (2014), https://www.nae.edu/111098/Geologic-Disposal-of-Spent-Nuclear-Fuel.
4. R. Becker, A. Forsström, Y. Yagodzinskyy, H. Hänninen, and M. Heikkilä, Sulphide-induced stress corrosion cracking and hydrogen absorption in copper exposed to sulphide and chloride containing deoxygenated water at 90°C, Report Number 2020:01 Strålsäkerhetsmyndigheten Swedish Radiation Safety Authority (2020) 1–50.
5. A. Forsström, R. Becker, H. Hänninen, Y. Yagodzinskyy, and M. Heikkilä, *Mater. Corros.*, **72**, 317 (2021).
6. C. M. Lousada, I. L. Soroka, Y. Yagodzinskyy, N. V. Tarakina, O. Todoshchenko, H. Hänninen, P. A. Korzhavyi, and M. Jonsson, *Sci. Rep.*, **6**, 24234 (2016).
7. Å. Martinsson and R. Sandström, *J. Mater. Sci.*, **47**, 6768 (2012).
8. Y. Yagodzinskyy, E. Malitckii, T. Saukkonen, and H. Hänninen, *Scr. Mater.*, **67**, 931 (2012).
9. A. Situm, B. Bahadormanesh, L. J. Bannenberg, F. Ooms, H. A. Feltham, G. Popov, M. Behazin, L. V. Goncharova, and J. J. Noël, *J. Electrochem. Soc.*, **170**, 041503 (2023).
10. H. Magnusson and K. Frisk, *Journal of Phase Equilibria and Diffusion*, **38**, 65 (2017).
11. S. Nakahara and Y. Okinaka, *Mater. Sci. Eng. A*, **101**, 227 (1988).
12. P. Sahiluoma, Y. Yagodzinskyy, S. Bossyut, and H. Hänninen, *J. Nucl. Mater.*, **574**, 154177 (2023).
13. J. Chen, Z. Qin, and D. W. Shoesmith, *Electrochim. Acta*, **56**, 7854 (2011).
14. J. Chen, Z. Qin, and D. W. Shoesmith, *J. Electrochem. Soc.*, **157**, C338 (2010).
15. M. Karlsson, L.-G. Johansson, L. Mazzei, J. Froitzheim, and M. Wolff, *ACS Materials Au*, **4**, 346 (2024).
16. H. M. Ha and H. Fritzsche, *J. Electrochem. Soc.*, **166**, C3064 (2019).
17. M. H. Wood, K. L. Browning, R. D. Barker, and S. M. Clarke, *J. Phys. Chem. B*, **120**, 5405 (2016).
18. H. Ha, H. Fritzsche, G. Burton, and J. Ulaganathan, *J. Electrochem. Soc.*, **164**, C699 (2017).
19. K. L. Cwalina, H. M. Ha, N. Ott, P. Reinke, N. Birbilis, and J. R. Scully, *J. Electrochem. Soc.*, **166**, C3241 (2019).
20. M. H. Wood, R. J. L. Welbourn, A. Zarbakhsh, P. Gutfreund, and S. M. Clarke, *Langmuir*, **31**, 7062 (2015).
21. A. Junghans, R. Chellappa, P. Wang, J. Majewski, G. Luciano, R. Marcelli, and E. Proietti, *Corros. Sci.*, **90**, 101 (2015).
22. K. Akutsu, T. Niizeki, S. Nagayama, N. Miyata, M. Sahara, A. Shimomura, M. Yoshii, and Y. Hasegawa, *J. Ceram. Soc. Jpn.*, **124**, 172 (2016).
23. R. J. Welbourn, C. Truscott, M. Skoda, A. Zarbakhsh, and S. Clarke, *Corros. Sci.*, **115**, 68 (2017).
24. S. Singh, A. Poswal, S. Ghosh, and S. Basu, *Pramana*, **71**, 1097 (2008).
25. D. Wlesler and C. Majkrzak, *MRS Online Proceedings Library (OPL)*, **376**, 247 (1994).
26. D. Wiesler and C. Majkrzak, *Physica B*, **198**, 181 (1994).
27. F. King and M. Behazin, *Corrosion and Materials Degradation*, **2**, 678 (2021).
28. A. Glavic and M. Björck, *J. Appl. Crystallogr.*, **55**, 1063 (2022).
29. S. Gotoh and Z. Takagi, *J. Nucl. Sci. Technol.*, **1**, 311 (1964).
30. M. A. Brocklebank, "High resolution ion beam investigations of the mechanisms of titanium anodization." *PhD Thesis*, Department of Physics and Astronomy, The University of Western Ontario (2018).
31. J. R. Tesmer and M. Nastasi, *Handbook of Modern Ion Beam Materials Analysis*, ed. J. C. Barbour, C.J. Maggiore, and J.W. Mayer (Materials Research Society, Pittsburgh, PA) (1995)1558992545 https://archive.org/details/handbookofmodern0000unse_k5q4.
32. W. Chu, J. Mayer, and M. Nicolet, *Backscattering Spectroscopy* (Academic Press, San Diego, CA) (1978), 1-12-173850-7.
33. E. Salehi Alaei, M. Guo, J. Chen, M. Behazin, E. Bergendal, C. Lilja, D. W. Shoesmith, and J. J. Noël, *Mater. Corros.*, **74**, 1690 (2023).
34. M. Guo, J. Chen, T. Martino, C. Lilja, J. A. Johansson, M. Behazin, W. J. Binns, P. G. Keech, J. J. Noël, and D. W. Shoesmith, *Mater. Corros.*, **72**, 300 (2021).
35. J. Chen, Z. Qin, L. Wu, J. J. Noël, and D. W. Shoesmith, *Corros. Sci.*, **87**, 233 (2014).
36. T. Martino, R. Partovi-Nia, J. Chen, Z. Qin, and D. W. Shoesmith, *Electrochim. Acta*, **127**, 439 (2014).
37. J. Halldin Stenlid, E. dos Santos, A. Johansson, and L. Pettersson, *Corros. Sci.*, **183**, 109313 (2021).
38. J. Chen, X. Pan, T. Martino, C. Lilja, M. Behazin, W. J. Binns, P. G. Keech, J. J. Noël, and D. W. Shoesmith, *Mater. Corros.*, **74**, 1665 (2023).
39. M. Vezvaie, J. Noël, Z. Tun, and D. Shoesmith, *J. Electrochem. Soc.*, **160**, C414 (2013).
40. J. Chen, Z. Qin, T. Martino, and D. Shoesmith, *Corros. Sci.*, **114**, 72 (2017).
41. B. Ibrahim, D. Zagidulin, M. Behazin, S. Ramamurthy, J. Wren, and D. Shoesmith, *Corros. Sci.*, **141**, 53 (2018).
42. F. King, C. Lilja, K. Pedersen, P. Pitkänen, and M. Vähänen, An update of the state-of-the-art report on the corrosion of copper under expected conditions in a deep geologic repository SKB TR-10-67 Swedish Nuclear Fuel and Waste Management Co., Solna, Sweden (2010), https://www.skb.com/publication/2202608/TR-10-67.pdf.
43. T. Martino, J. Chen, J. Noël, and D. Shoesmith, *Electrochim. Acta*, **331**, 135319 (2020).